Uplink Performance Analysis of Dense Cellular Networks with LoS and NLoS Transmissions

Tian Ding, *Student Member, IEEE*, Ming Ding, *Member, IEEE*,

Guoqiang Mao, *Senior Member, IEEE*, Zihuai Lin, *Senior Member, IEEE*,

David López-Pérez, *Member, IEEE*, Albert Zomaya, *Fellow, IEEE*

Abstract—In this paper, we analyse the coverage probability and the area spectral efficiency (ASE) for the uplink (UL) of dense small cell networks (SCNs) considering a practical path loss model incorporating both line-of-sight (LoS) and non-line-of-sight (NLoS) transmissions. Compared with the existing work, we adopt the following novel approaches in our study: (i) we assume a practical user association strategy (UAS) based on the smallest path loss, or equivalently the strongest received signal strength; (ii) we model the positions of both base stations (BSs) and the user equipments (UEs) as two independent Homogeneous Poisson point processes (HPPPs); and (iii) the correlation of BSs' and UEs' positions is considered, thus making our analytical results more accurate. The performance impact of LoS and NLoS transmissions on the ASE for the UL of dense SCNs is shown to be significant, both quantitatively and qualitatively, compared with existing work that does not differentiate LoS and NLoS transmissions. In particular, existing work predicted that a larger UL power compensation factor would always result in a better ASE in the practical range of BS density, i.e., $10^1 \sim 10^3$ BSs/km^2. However, our results show that a smaller UL power compensation factor can greatly boost the ASE in the UL of dense SCNs, i.e., $10^2 \sim 10^3$ BSs/km^2,

Tian Ding is with The University of Technology Sydney, Australia (e-mail: Tian.Ding@student.uts.edu.au).

Ming Ding is with Data61, Sydney, Australia (e-mail: Ming.Ding@nicta.com.au).

Guoqiang Mao is with the School of Computing and Communication, The University of Technology Sydney, Australia. He also holds adjunct positions at the School of Electronic Information & Communications, Huazhong University of Science & Technology, Wuhan, China, and the School of Information and Communication Engineering, Beijing University of Posts and Telecommunications, Beijing, China (e-mail: g.mao@ieee.org). Guoqiang Mao's research is supported by Australian Research Council (ARC) Discovery project DP110100538 and Chinese National Science Foundation project 61428102.

Zihuai Lin is with the School of Electrical and Information Engineering, The University of Sydney, Australia (e-mail: zihuai.lin@sydney.edu.au).

David López-Pérez is with Bell Labs, Nokia, Dublin, Ireland (email: dr.david.lopez@ieee.org).

Albert Zomaya is with the School of IT, the University of Sydney, Australia (email: albert.zomaya@sydney.edu.au).

while a larger UL power compensation factor is more suitable for sparse SCNs, i.e., $10^1 \sim 10^2$ BSs/km^2.

Index Terms—dense small cell networks (SCNs), Uplink (UL), Line-of-Sight (LoS), Non-Line-of-Sight (NLoS), coverage probability, area spectral efficiency (ASE)

I. INTRODUCTION

By means of network densification, small cell networks (SCNs) can achieve a high spatial reuse gain, which further leads to a high network capacity [1]. Particularly, the orthogonal deployment of SCNs within the existing macrocell network, i.e., small cells and macrocells operating on different frequency spectrum (Small Cell Scenario #2a defined in [2]), is prioritized in the design of the 4th generation (4G) Long Term Evolution (LTE) networks by the 3rd Generation Partnership Project (3GPP). Furthermore, dense SCNs are envisaged to be the workhorse for capacity enhancement in the 5th generation (5G) networks due to its large performance gains and easy deployment [1], [3], [4]. Thus, this paper focuses on studying the performance of these orthogonal deployments of dense SCNs.

In our previous work [5], we conducted a study on the downlink (DL) of dense SCNs considering a sophisticated path loss model that differentiates line-of-sight (LoS) and non-line-of-sight (NLoS) transmissions. LoS transmission may occur when the distance between a transmitter and a receiver is small, and NLoS transmission is more common in office environments and in central business districts. Moreover, the probability that there exists a LoS path between the transmitter and the receiver increases as their distance decreases. It is observed in [5] that the reduction of the distance between the transmitter and the receiver as the density of small cell base stations (BSs) increases will cause a transition from NLoS transmission to LoS transmission,

which has a significant impact, both quantitatively and qualitatively, on the performance of DL dense SCNs. Motivated by this finding [5], in this paper, we continue to query whether such NLoS-to-LoS transitions may significantly affect the performance of uplink (UL) dense SCNs.

Our work distinguishes from existing work [5], [6], [7] on the performance analysis of UL dense SCNs in three major aspects. First, we assume a user association strategy (UAS) that each UE is associated with the BS with the smallest path loss to the UE, or equivalently each UE is associated with the BS that delivers the strongest received signal strength [5]. Note that in our previous work [7] and existing work in the literature [6], the authors assumed that each UE should be associated with the closest BS. Such assumption is not appropriate for the realistic path loss model with LoS and NLoS transmissions, because in practice it is possible for a UE to associate with a BS that is not the closest one but with a LoS path, instead of the nearest BS with a NLoS path. Second, we assume that the BSs and the UEs are deployed according to two independent Homogeneous Poisson point processes (HPPPs), which is more practical and realistic compared with the previous work [6], [7]. Third, we consider the correlation of BS and UE positions explained later in the paper, thus making our numerical results more accurate than the previous work [6], which ignored such correlation. The main contributions of this paper are as follows:

- Numerically tractable results are obtained for the UL coverage probability and the UL area spectral efficiency (ASE) performance using a piecewise path loss model, incorporating both LoS and NLoS transmissions.
- Our theoretical analysis of the UL of dense SCNs shows a similar performance trend that was found for the DL of dense SCNs in our previous work [5], i.e., when the density of UEs is larger than a threshold, the ASE may suffer from a slow growth or even a decrease. Then, the ASE will grow almost linearly as the UE density increases above another larger threshold. This finding is in stark contrast with previous results using a simplistic path loss model that does not differentiate LoS and NLoS transmissions [6].
- Our theoretical analysis also indicates that the performance impact of LoS and NLoS trans-

missions on the UL of SCNs with *UL power compensation* is significant both quantitatively and qualitatively compared with existing work in the literature that does not differentiate LoS and NLoS transmissions. The details of the UL power compensation scheme will be introduced in Section III. In particular, the previous work [6] showed that a larger UL power compensation factor should always deliver a better ASE performance in the practical range of BS density, i.e., $10^1 \sim 10^3$ BSs/km^2. However, our results show that a smaller UL power compensation factor can greatly boost the ASE performance in dense SCNs, i.e., $10^2 \sim 10^3$ BSs/km^2, while a larger UL power compensation factor is more suitable for sparse SCNs, i.e., $10^1 \sim 10^2$ BSs/km^2. Our new finding indicates that it is possible to save UE battery and meanwhile obtain a high ASE in the UL of dense SCNs in 5G, if the UL power compensation factor is optimized.

The remainder of this paper is structured as follows. Section II compares the closest related work to our work. Section III describes the system model. Section IV presents our main analytical results on the UL coverage probability and the UL ASE. Section V presents the application of our main analytical results on the UL coverage probability and the UL ASE in a 3GPP special case, followed by a more efficient computation method to evaluate the results using the Gauss-Laguerre quadrature. The numerical results and simulation results are discussed in Section VI. Finally, the conclusions are drawn in Section VII.

II. RELATED WORK

In the DL performance analysis of cellular networks based on stochastic geometry, BS positions are typically modeled as a Homogeneous Poisson point process (HPPP) on the plane [8], and in this case, the coverage probability can be expressed in a closed-form. Furthermore, an important and novel capacity model was proposed for HPPP random cellular networks, where the impact of random interference on the cooperative communications is analyzed by a closed-form expression [9]. In the UL performance analysis of cellular networks based on stochastic geometry, UE positions are typically modeled as a HPPP on the plane [6], and BS positions are

assumed to be uniformly and randomly deployed in the Voronoi cell of each UE. The difficulty of modeling both BSs and UEs as a HPPP is that the BS and UE positions are coupled [6], [10], and the dependence of UE positions is therefore hard to analyse [11], [12], [13]. Such dependence occurs because if a UE is associated with a BS that delivers the strongest received signal (or is closest to the UE), it implies that there are no other BSs that can be located in positions that deliver the strongest received signal (or in a closer distance than the aforementioned BS). To derive tractable and closed-form results, previous work ignored this dependence and modeled the distance between a UE and its associated BS as an independent identical distributed (i.i.d.) random variable.

In greater detail, in [6], the authors assumed that the UEs are randomly distributed following a HPPP, and exactly one BS is randomly and uniformly located in each UE's Voronoi cell, i.e., each BS associates with its nearest UE. It is also assumed that the distance between each BS and its serving UE is i.i.d. Rayleigh distributed. The system model of only deploying UEs as a HPPP [6] makes it difficult to conduct network performance analysis for UL of SCNs. Furthermore, the association strategy that each BS associates with its nearest UE [6] is impractical, and the assumption that all of the BS-UE association distances are i.i.d. Rayleigh distributed [6] is unrealistic.

In [14], the authors considered UE spatial blocking, which is referred to as the outage caused by limited number of usable channels, and derived approximate expressions for the UL blocking probability and the UL coverage probability. In [15], the authors proposed a tractable model to characterize the UL rate distribution in a K-tier heterogeneous cellular networks (HCNs) considering power control and load balancing. In [16], the authors considered the maximum power limitation for UEs and obtained approximate expressions for the UL outage probability and UL spectral efficiency. However, none of the aforementioned UL related work considered a realistic path loss model with line-of-sight (LoS) and non-line-of-sight (NLoS) transmissions. In contrast, in this paper, we consider a sophisticated path loss model incorporating both LoS and NLoS transmissions to study their performance impact on dense SCNs and show that LoS and NLoS transmissions have a significant impact on the performance of UL

dense SCNs.

LoS and NLoS transmissions have been previously investigated in the DL performance analysis of dense SCNs [5], [17]. One major conclusion of [5] is that the ASE performance will slowly increase or even decrease in certain BS density regions. It is interesting to see whether this conclusion holds for UL dense SCNs. In our previous work on the UL performance analysis of dense SCNs [7], we assume that each UE is associated with its nearest BS, which may not be a practical assumption when considering LoS and NLoS transmissions. Compared with [7], in this work we consider a more realistic user association strategy, in which a UE associates with the BS that has the smallest path loss, or equivalently delivers the strongest received signal strength. This user association strategy is more realistic and is particularly important when considering both LoS and NLoS transmissions that are present in realistic radio environment, because the closest BS may possibly have only a NLoS path to the UE and therefore may offer a weaker signal than a BS that is further away but has a LoS path to the UE.

III. SYSTEM MODEL

Different from the assumption that only UEs' deployment follows HPPP distribution [6], in this paper, we assume that both BSs and UEs are distributed following HPPPs with densities λ BSs/km^2 and λ^{UE} UEs/km^2, respectively. Here, we assume that $\lambda^{\mathrm{UE}} \gg \lambda$ so that all the BSs are activated to serve at least one UE. Each UE is assumed to associate with the BS with the smallest path loss. We focus on UL and consider a randomly tagged BS, which is denoted as the typical BS located at the origin. With the assumption of $\lambda^{\mathrm{UE}} \gg \lambda$, on each time-frequency resource block, each BS has one active UE in its coverage area. The UE associated with the typical BS is denoted as the typical UE, and the other UEs using the same time-frequency resource block are denoted as the interfering UEs. The distance from the typical UE to the typical BS is denoted by R, which is a random variable whose distribution will be analyzed later. Throughout the paper, we use the upper case letters, e.g., R, to denote a random variable and use the lower case letters, e.g., r, to denote specific instance of the random variable.

The link from the typical UE to the typical BS has a LoS path or a NLoS path with probability $\Pr^L(r)$ and $1 - \Pr^L(r)$, respectively, where such probability can be computed by the following piecewise function [5],

$$\Pr^L(r) = \begin{cases} \Pr_1^L(r), & 0 < r \leq d_1 \\ \Pr_2^L(r), & d_1 < r < d_2 \\ \vdots & \vdots \\ \Pr_N^L(r), & r > d_{N-1} \end{cases}. \quad (1)$$

The distance dependent path loss is expressed as $\zeta(r)$ with r being the distance, and the path loss gain is $\zeta(r)^{-1}$, where the path loss of each link is modeled as (2), which is shown on the top of next page.

In (2), for $n \in \{1, 2, \cdots, N\}$, A_n^L is the path loss of LoS path at a reference distance of $r = 1$, A_n^{NL} is the path loss of NLoS path at a reference distance of $r = 1$, α_n^L is the path loss exponent of LoS link, and α_n^{NL} is the path loss exponent of NLoS link.

The UL transmission power of UE k located at a distance of r is denoted by P_k, and is subject to a semi-static power control (PC) mechanism, i.e., the fractional path loss compensation (FPC) scheme [18]. Based on this FPC scheme, P_k is modeled as

$$P_k = P_0 \zeta(r)^\epsilon, \quad (3)$$

where P_0 is the baseline power on the considered RB at the UE, $\epsilon \in (0, 1]$ is the FPC factor, and $\zeta(r)$ is expressed in (2).

In (3), the distance-based fractional power compensation term $\zeta(r)^\epsilon$ is denoted by $\beta(r)$ and written as

$$\beta(r) = \zeta(r)^\epsilon. \quad (4)$$

Therefore, the received signal power at the typical BS can be written as

$$\begin{aligned} P^{sig} &= P_0 \beta(R) \zeta(R)^{-1} g \\ &= P_0 \zeta(R)^{(\epsilon-1)} g, \end{aligned} \quad (5)$$

where g denotes the channel gain of the multi-path fading channel and is an i.i.d. exponential distributed random variable. Hence, g follows an exponential distribution with unit mean.

As a result, the SINR at the typical BS of the typical UE can be expressed as

$$\text{SINR} = \frac{P^{sig}}{\sigma^2 + I_Z}, \quad (6)$$

where σ^2 is the noise power, Z is the set of interfering UEs, and I_Z is the interference given by

$$I_Z = \sum_Z P_0 \beta(R_z) \zeta(D_z)^{-1} g_z, \quad (7)$$

where g_z denotes the channel gain of the multi-path fading channel of interferer $z \in Z$, and is an i.i.d. exponential distributed random variable, which follows an exponential distribution with unit mean. The distance of interferer $z \in Z$ to its serving BS is denoted by R_z, and the distance of interferer $z \in Z$ to the typical BS is denoted by D_z. The details of the distribution of R_z and R are given in Section V. Since $D_z \gg R_z$, D_z can be approximated by the distance from the serving BS of interferer z to the typical BS.

IV. ANALYSIS BASED ON THE PROPOSED PATH LOSS MODEL

The UL coverage probability for the typical BS can be formulated as

$$P^{cov}(\lambda, T) = \Pr[\text{SINR} > T], \quad (8)$$

where T is the SINR threshold.

The area spectral efficiency (ASE) in bps/Hz/km^2 for a given λ can be formulated as [5]

$$A^{ASE}(\lambda, T_0) = \lambda \int_{T_0}^{\infty} \log_2(1+x) f_X(\lambda, x) \, dx, \quad (9)$$

where T_0 is the minimum working SINR for the considered SCN, and $f_X(\lambda, x)$ is the PDF of the SINR observed at the typical BS for a particular value of λ.

Based on the definition of $P^{cov}(\lambda, T)$, which is the complementary cumulative distribution function (CCDF) of SINR, $f_X(\lambda, x)$ can be computed as

$$f_X(\lambda, x) = \frac{\partial(1 - P^{cov}(\lambda, x))}{\partial x}. \quad (10)$$

Based on the system model presented in Section III, we can calculate $P^{cov}(\lambda, T)$ and present it in the following theorem.

Theorem 1. $P^{cov}(\lambda, T)$ *can be derived as*

$$P^{cov}(\lambda, T) = \sum_{n=1}^{N} \left(T_n^L + T_n^{NL} \right), \quad (11)$$

where

$$T_n^L = \int_{d_{n-1}}^{d_n} Pr \left[\frac{P_0 g \left(A^L r^{\alpha^L} \right)^{(\epsilon-1)}}{\sigma^2 + I_Z} > T \middle| LoS \right] f_{R,n}^L(r) dr,$$

$$T_n^{NL} = \int_{d_{n-1}}^{d_n} Pr \left[\frac{P_0 g \left(A^{NL} r^{\alpha^{NL}} \right)^{(\epsilon-1)}}{\sigma^2 + I_Z} > T \middle| NLoS \right] f_{R,n}^{NL}(r) dr,$$

$$(12)$$

$$\zeta(r) = \begin{cases} \begin{cases} A_1^{\mathrm{L}} r^{\alpha_1^{\mathrm{L}}}, & \text{LoS with probability } \mathrm{Pr}_1^{\mathrm{L}}(r) \\ A_1^{\mathrm{NL}} r^{\alpha_1^{\mathrm{NL}}}, & \text{NLoS with probability } \left(1 - \mathrm{Pr}_1^{\mathrm{L}}(r)\right) \end{cases}, & 0 < r \le d_1 \\ \begin{cases} A_2^{\mathrm{L}} r^{\alpha_2^{\mathrm{L}}}, & \text{LoS with probability } \mathrm{Pr}_2^{\mathrm{L}}(r) \\ A_2^{\mathrm{NL}} r^{\alpha_2^{\mathrm{NL}}}, & \text{NLoS with probability } \left(1 - \mathrm{Pr}_2^{\mathrm{L}}(r)\right) \end{cases}, & d_1 < r < d_2 \\ \vdots & \vdots \\ \begin{cases} A_N^{\mathrm{L}} r^{\alpha_N^{\mathrm{L}}}, & \text{LoS with probability } \mathrm{Pr}_N^{\mathrm{L}}(r) \\ A_N^{\mathrm{NL}} r^{\alpha_N^{\mathrm{NL}}}, & \text{NLoS with probability } \left(1 - \mathrm{Pr}_N^{\mathrm{L}}(r)\right) \end{cases}, & r > d_{N-1} \end{cases} \tag{2}$$

and d_0 and d_N are respectively defined as 0 and ∞. Moreover, $f_{R,n}^{L}(r)$ and $f_{R,n}^{NL}(r)$ can be respectively derived as

$$\begin{aligned} & f_{R,n}^{L}(r) \\ & = \exp\left(-\int_0^{r_1}\left(1 - Pr_n^{\mathrm{L}}(u)\right)2\pi u\lambda du\right) \\ & \quad \times \exp\left(-\int_0^{r} Pr_n^{\mathrm{L}}(u) 2\pi u\lambda du\right) \\ & \quad \times Pr_n^{\mathrm{L}}(r) 2\pi r\lambda, \quad (d_{n-1} < r < d_n), \end{aligned} \tag{13}$$

and

$$\begin{aligned} & f_{R,n}^{NL}(r) \\ & = \exp\left(-\int_0^{r_2} Pr_n^{\mathrm{L}}(u) 2\pi u\lambda du\right) \\ & \quad \times \exp\left(-\int_0^{r}\left(1 - Pr_n^{\mathrm{L}}(u)\right)2\pi u\lambda du\right) \\ & \quad \times \left(1 - Pr_n^{\mathrm{L}}(r)\right) 2\pi r\lambda, \quad (d_{n-1} < r < d_n), \end{aligned} \tag{14}$$

where r_1 and r_2 are determined respectively by

$$r_1 = \left(A^L r^{\alpha^L}/A^{NL}\right)^{1/\alpha^{NL}}, \tag{15}$$

and

$$r_2 = \left(A^{NL} r^{\alpha^{NL}}/A^L\right)^{1/\alpha^L}. \tag{16}$$

Furthermore, $\Pr\left[\left.\dfrac{P_0 g \left(A^L r^{\alpha^L}\right)^{(\epsilon-1)}}{\sigma^2+I_Z} > T\right| LoS\right]$ *and* $\Pr\left[\left.\dfrac{P_0 g \left(A^{NL} r^{\alpha^{NL}}\right)^{(\epsilon-1)}}{\sigma^2+I_Z} > T\right| NLoS\right]$ *are respectively computed by*

$$\begin{aligned} & \Pr\left[\left.\frac{P_0 g \left(A^L r^{\alpha^L}\right)^{(\epsilon-1)}}{\sigma^2+I_Z} > T\right| LoS\right] \\ & = \exp\left(-\frac{T\sigma^2}{P_0\left(A^L r^{\alpha^L}\right)^{(\epsilon-1)}}\right) \mathscr{L}_{I_Z}\left(\frac{T}{P_0\left(A^L r^{\alpha^L}\right)^{(\epsilon-1)}}\right), \end{aligned} \tag{17}$$

and

$$\begin{aligned} & \Pr\left[\left.\frac{P_0 g \left(A^{NL} r^{\alpha^{NL}}\right)^{(\epsilon-1)}}{\sigma^2+I_Z} > T\right| NLoS\right] \\ & = \exp\left(-\frac{T\sigma^2}{P_0\left(A^{NL} r^{\alpha^{NL}}\right)^{(\epsilon-1)}}\right) \mathscr{L}_{I_Z}\left(\frac{T}{P_0\left(A^{NL} r^{\alpha^{NL}}\right)^{(\epsilon-1)}}\right), \end{aligned} \tag{18}$$

where $\mathscr{L}_{I_Z}(s)$ is the Laplace transform of RV I_Z evaluated at s.

Proof: See Appendix A. ■

As can be observed from Theorem 1, the piece-wise path loss function for LoS transmission, the piece-wise path loss function for NLoS transmission, and the piece-wise LoS probability function play active roles in determining the final result of $P^{\mathrm{cov}}(\lambda, T)$. We will investigate their impacts on network performance in detail in the following sections. Plugging $P^{\mathrm{cov}}(\lambda, T)$ obtained from (11) into (10), we can get the result of the ASE using (9).

V. STUDY OF A 3GPP SPECIAL CASE

As a special case for Theorem 1, we consider a path loss function adopted in the 3GPP as [18]

$$\zeta(r) = \begin{cases} A^{\mathrm{L}} r^{\alpha^{\mathrm{L}}}, & \text{LoS with probability } \mathrm{Pr}^{\mathrm{L}}(r) \\ A^{\mathrm{NL}} r^{\alpha^{\mathrm{NL}}}, & \text{NLoS with probability } \left(1 - \mathrm{Pr}^{\mathrm{L}}(r)\right) \end{cases}, \tag{19}$$

together with a linear LoS probability function of $\mathrm{Pr}^L(r)$, defined in the 3GPP as [19]

$$\mathrm{Pr}^{\mathrm{L}}(r) = \begin{cases} 1 - \frac{r}{d_1}, & 0 < r \le d_1 \\ 0, & r > d_1 \end{cases}, \tag{20}$$

where d_1 is the cut-off distance of the LoS link. For the 3GPP special case, according to Theorem 1, $P^{\mathrm{cov}}(\lambda, \gamma)$ can then be computed by

$$P^{\mathrm{cov}}(\lambda, T) = \sum_{n=1}^{2}\left(T_n^{\mathrm{L}} + T_n^{\mathrm{NL}}\right). \tag{21}$$

In the following subsections, we will investigate the results of T_1^{L}, T_1^{NL}, T_2^{L}, and T_2^{NL}, respectively.

A. The Result of T_1^{L}

Regarding the result of T_1^{L}, which is the coverage probability when the typical UE is associated with the typical BS with a LoS link of distance less than d_1, we present Lemma 2 in the following.

Lemma 2. *When the typical UE is associated with a LoS BS of a distance less than d_1, the coverage probability T_1^{L} can be computed by*

$$T_1^{\mathrm{L}} = \int_0^{d_1} e^{-\frac{T\sigma^2}{P_0\left(A^L r^{\alpha^L}\right)^{(\epsilon-1)}}} \mathscr{L}_{I_Z}\left(\frac{T}{P_0\left(A^L r^{\alpha^L}\right)^{(\epsilon-1)}}\right) f_{R,1}^L(r) dr,$$
(22)

where

$$f_{R,1}^L(r) = \exp\left(-\pi\lambda r^2 + 2\pi\lambda\left(\frac{r^3}{3d_1} - \frac{r_1^3}{3d_1}\right)\right)\left(1 - \frac{r}{d_1}\right) 2\pi r\lambda,$$
(23)

and the Laplace transform $\mathscr{L}_{I_Z}(s)$ is expressed as

$$
\begin{aligned}
&\mathscr{L}_{I_Z}(s) \\
&= \exp\left\{-2\pi\lambda \int_r^{d_1}\left(1 - \frac{x}{d_1}\right)\right. \\
&\quad \left. \times \int_0^\infty \left(\frac{1}{1 + s^{-1}P_0^{-1}\beta(u)^{-1}\zeta(x)} f_{R_z}^{1L}(u)\, du \middle| LoS\right) x dx\right\} \\
&\quad \times \exp\left\{-2\pi\lambda \int_{r_1}^{d_1}\left(\frac{x}{d_1}\right)\right. \\
&\quad \left. \times \int_0^\infty \left(\frac{1}{1 + s^{-1}P_0^{-1}\beta(u)^{-1}\zeta(x)} f_{R_z}^{1NL}(u)\, du \middle| NLoS\right) x dx\right\} \\
&\quad \times \exp\left\{-2\pi\lambda \int_{d_1}^\infty 1\right. \\
&\quad \left. \times \int_0^\infty \left(\frac{1}{1 + s^{-1}P_0^{-1}\beta(u)^{-1}\zeta(x)} f_{R_z}^{2NL}(u)\, du \middle| NLoS\right) x dx\right\}.
\end{aligned}
$$
(24)

According to the HPPP system model, the distribution of R_z is the same as R, but bounded by x. The PDF of R_z can be written as

$$f_{R_z}(u) = \begin{cases} f_{R_z,1}^L(u), & LoS, \ 0 < u \le x \\ f_{R_z,1}^{1NL}(u), & NLoS, \ 0 < u \le x_1 \\ f_{R_z,1}^{2NL}(u), & NLoS, \ y_1 < u \le d_1 \\ f_{R_z,2}^{NL}(u), & NLoS, \ d_1 < u \le x \end{cases},$$
(25)

where

$$f_{R_z,1}^L(u) = \exp\left(-\pi\lambda u^2 + 2\pi\lambda\left(\frac{u^3}{3d_1} - \frac{u_1^3}{3d_1}\right)\right) \times \left(1 - \frac{u}{d_1}\right) 2\pi u\lambda,$$
(26)

$$f_{R_z,1}^{1NL}(u) = \exp\left(-\pi\lambda u_2^2 + 2\pi\lambda\left(\frac{u_2^3}{3d_1} - \frac{u^3}{3d_1}\right)\right) \times \left(\frac{u}{d_1}\right) 2\pi u\lambda,$$
(27)

$$f_{R_z,1}^{2NL}(u) = \exp\left(2\pi\lambda\left(-\frac{d_1^2}{6} - \frac{u^3}{3d_1}\right)\right)\left(\frac{u}{d_1}\right) 2\pi u\lambda,$$
(28)

and

$$f_{R_z,2}^{NL}(u) = \exp\left(-\pi\lambda u^2\right) 2\pi u\lambda,$$
(29)

where

$$u_1 = \left(A^L u^{\alpha^L}/A^{NL}\right)^{1/\alpha^{NL}},$$
(30)

and

$$u_2 = \left(A^{NL} u^{\alpha^{NL}}/A^L\right)^{1/\alpha^L},$$
(31)

Specifically, when the interference comes from a LoS path, $f_{R_z}^{1L}(u)$ can be derived as

$$f_{R_z}^{1L}(u) = \begin{cases} f_{R_z,1}^L(u), & LoS, \ 0 < u \le x \\ f_{R_z,1}^{1NL}(u), & NLoS, \ 0 < u \le x_1 \end{cases},$$
(32)

where

$$x_1 = \left(A^L x^{\alpha^L}/A^{NL}\right)^{1/\alpha^{NL}}.$$
(33)

Conditioned on $x \le d_1$, when the interference path is NLoS, $f_{R_z}^{1NL}(u)$ can be derived as

$$f_{R_z}^{1NL}(u) = \begin{cases} \begin{cases} f_{R,1}^L(u), & LoS, & 0 < u \le x_2 \\ f_{R,1}^{1NL}(u), & NLoS, & 0 < u \le x \end{cases}, & r_1 < x \le y_1 \\ \begin{cases} f_{R,1}^L(u), & LoS, & 0 < u \le d \\ f_{R,1}^{1NL}(u), & NLoS, & 0 < u \le y_1 \\ f_{R,1}^{2NL}(u), & NLoS, & y_1 < u \le x \end{cases}, & y_1 < x \le d_1 \end{cases},$$
(34)

where

$$y_1 = \left(A^L d_1^{\alpha^L}/A^{NL}\right)^{1/\alpha^{NL}},$$
(35)

and

$$x_2 = \left(A^{NL} x^{\alpha^{NL}}/A^L\right)^{1/\alpha^L}.$$
(36)

Conditioned on $x > d_1$, when the interference path is NLoS, $f_{R_z}^{2NL}(u)$ can be derived as

$$f_{R_z}^{2NL}(u) = \begin{cases} f_{R_z,1}^L(u), & LoS, \ 0 < u \le d_1 \\ f_{R_z,1}^{1NL}(u), & NLoS, \ 0 < u \le y_1 \\ f_{R_z,}^{2NL}(u), & NLoS, \ y_1 < u \le d_1 \\ f_{R_z,2}^{NL}(u), & NLoS, \ d_1 < u \le x \end{cases}.$$
(37)

Proof: See Appendix B. ∎

B. The Result of T_1^{NL}

Regarding the result of T_1^{NL}, which is the coverage probability when the typical UE is associated with the typical BS with a NLoS link of distance less than d_1, we propose Lemma 3 in the following.

Lemma 3. T_1^{NL} *can be derived as*

$$T_1^{NL} = \int_0^{d_1} e^{-\frac{T\sigma^2}{P_0 r^{\alpha^{NL}(\epsilon-1)}}} \mathscr{L}_{I_Z}\left(\frac{T}{P_0 r^{\alpha^{NL}(\epsilon-1)}}\right) f_{R,1}^{NL}(r)\, dr, \tag{38}$$

where

$$f_{R,1}^{NL}(r)$$
$$= \begin{cases} \exp\left(-\pi\lambda r_2^2 + 2\pi\lambda\left(\frac{r_2^3}{3d_1} - \frac{r^3}{3d_1}\right)\right) \\ \quad \times \left(\frac{r}{d_1}\right) 2\pi r\lambda, & 0 < r \le y_1 \\ \exp\left(-\frac{\pi\lambda d_1^2}{3} - \frac{2\pi\lambda r^3}{3d_1}\right) \\ \quad \times \left(\frac{r}{d_1}\right) 2\pi r\lambda, & y_1 < r \le d_1 \end{cases}, \tag{39}$$

and the Laplace transform $\mathscr{L}_{I_Z}(s)$ for $0 < r \le y_1$ and $y_1 < r \le d_1$ are respectively expressed as

$$\mathscr{L}_{I_Z}(s)$$
$$= \exp\left(-2\pi\lambda \int_{r_2}^{d_1}\left(1 - \frac{x}{d_1}\right)\right.$$
$$\left. \times \int_0^\infty \left(\frac{1}{1 + s^{-1}P_0^{-1}\beta(u)^{-1}\zeta(x)} f_{R_z}^{1L}(u)\, du\Big| LoS\right) x\, dx\right)$$
$$\times \exp\left(-2\pi\lambda \int_r^{d_1}\left(\frac{x}{d_1}\right)\right.$$
$$\left. \times \int_0^\infty \left(\frac{1}{1 + s^{-1}P_0^{-1}\beta(u)^{-1}\zeta(x)} f_{R_z}^{1NL}(u)\, du\Big| NLoS\right) x\, dx\right)$$
$$\times \exp\left(-2\pi\lambda \int_{d_1}^\infty 1\right.$$
$$\left. \times \int_0^\infty \left(\frac{1}{1 + s^{-1}P_0^{-1}\beta(u)^{-1}\zeta(x)} f_{R_z}^{2NL}(u)\, du\Big| NLoS\right) x\, dx\right), \tag{40}$$

and

$$\mathscr{L}_{I_Z}(s)$$
$$= \exp\left(-2\pi\lambda \int_r^{d_1} \frac{x}{d_1}\right.$$
$$\left. \times \int_0^\infty \left(\frac{1}{1 + s^{-1}P_0^{-1}\beta(u)^{-1}\zeta(x)} f_{R_z}^{1NL}(u)\, du\Big| NLoS\right) x\, dx\right)$$
$$\times \exp\left(-2\pi\lambda \int_{d_1}^\infty 1\right.$$
$$\left. \times \int_0^\infty \left(\frac{1}{1 + s^{-1}P_0^{-1}\beta(u)^{-1}\zeta(x)} f_{R_z}^{2NL}(u)\, du\Big| NLoS\right) x\, dx\right), \tag{41}$$

where $r_2 = \left(A^L r^{\alpha^{NL}}/A^{NL}\right)^{1/\alpha^L}$.

Proof: The proof is very similar to that in Appendix B. Thus it is omitted for brevity. ∎

C. The Result of T_2^L

The result of T_2^{L} is the coverage probability when the typical UE is associated with the typical BS with a LoS link of distance larger than d_1. From Theorem 1, T_2^{L} can be derived as

$$T_2^L = \int_{d_1}^\infty \Pr\left[\frac{P_0 g\left(A^L r^{\alpha^L}\right)^{(\epsilon-1)}}{\sigma^2 + I_Z} > T\,\Big|\, LoS\right] f_{R,2}^L(r) dr. \tag{42}$$

According to Theorem 1 and (20), $f_{R,2}^L(r)$ can be calculated by

$$f_{R,2}^L(r)$$
$$= \exp\left(-\int_0^{r_1}\left(1 - \Pr^L(u)\right)2\pi u\lambda du\right)$$
$$\quad \times \exp\left(-\int_0^r \Pr^L(u)\,2\pi u\lambda du\right) \times 0 \times 2\pi r\lambda$$
$$= 0, \quad (r > d_1). \tag{43}$$

Plugging (43) into (42), yields

$$T_2^L = 0. \tag{44}$$

D. The Result of T_2^{NL}

Regarding the result of T_2^{NL}, which is the coverage probability when the typical UE is associated with the typical BS with a NLoS link of distance larger than d_1, we propose Lemma 4 in the following.

Lemma 4. T_2^{NL} *can be derived as*

$$T_2^{NL} = \int_{d_1}^\infty e^{-\frac{T\sigma^2}{P_0 r^{\alpha^{NL}(\epsilon-1)}}} \mathscr{L}_{I_Z}\left(\frac{T}{P_0 r^{\alpha^{NL}(\epsilon-1)}}\right) f_{R,2}^{NL}(r)\, dr, \tag{45}$$

where

$$f_{R,2}^{NL}(r) = \exp\left(-\pi\lambda r^2\right) 2\pi r\lambda, \tag{46}$$

and the Laplace transform $\mathscr{L}_{I_Z}(s)$ is expressed as

$$\mathscr{L}_{I_Z}(s)$$
$$= \exp\left(-2\pi\lambda \int_r^\infty 1\right.$$
$$\left. \times \int_0^\infty \left(\frac{1}{1 + s^{-1}P_0^{-1}\beta(u)^{-1}\zeta(x)} f_{R_z}^{2NL}(u)\, du\Big| NLoS\right) x\, dx\right). \tag{47}$$

Proof: The proof is very similar to that in Appendix B. Thus it is omitted for brevity.. ∎

E. Evaluation Using the Gauss-Laguerre Quadrature

To improve the tractability of the derived results, we propose to approximate the infinite integral of outer-most integrals in (45) by the Gauss-Laguerre quadrature [20], expressed as

$$\int_0^\infty f(u)\, e^{-u} du \approx \sum_{i=1}^n \omega_i f(u_i), \tag{48}$$

where n is the degree of Laguerre polynomial, and u_i and ω_i are the i-th abscissas and weight

of the quadrature. For practical use, n should be set to a value above 10 to ensure good numerical accuracy [20].

To utilize the Gauss-Laguerre quadrature, the outermost integral in (45) is rewritten by using the change of variable $\tilde{r} = \pi\lambda r^2$. To evaluate (45) by means of the Gauss-Laguerre quadrature, we propose Lemma 5 in the following.

Lemma 5. *By using the Gauss-Laguerre quadrature as shown in (48), (45) can be approximated and simplified as*

$$
\begin{aligned}
& T_2^{NL} \\
& \approx \sum_{i=1}^{n} \omega_i \exp\left(-\frac{T\sigma^2}{P_0\left(\sqrt{\left[u_i+\pi\lambda(d_1)^2\right](\pi\lambda)^{-1}} \right)^{\alpha^{NL}(\epsilon-1)}} \right. \\
& \left. -\pi\lambda\left(d_1\right)^2 \right) \\
& \times \mathscr{L}_{I_Z}\left(\frac{T}{P_0\sqrt{\left[u_i+\pi\lambda(d_1)^2\right](\pi\lambda)^{-1}}^{\alpha^{NL}(\epsilon-1)}} \right).
\end{aligned}
$$

(49)

Proof: See Appendix C. ∎

Thanks to Lemma 5, the 3-fold integral computation in (45) can now be simplified as a 2-fold integral computation, which improves the tractability of our results.

VI. SIMULATION AND DISCUSSION

In this section, we present numerical and simulation results to establish the accuracy of our analysis and further study the performance of the UL of dense SCNs. We adopt the following parameters according to the 3GPP recommendations [18], [21]: $d_1 = 0.3$ km, $\alpha^L = 2.09$, $\alpha^{NL} = 3.75$, $P_0 = $ -76 dBm, $\sigma^2 = $ -99 dBm (with a noise figure of 5 dB at each BS). We first consider a sparse network in subsection VI-A, and then we analyze a dense network in the subsections VI-B and VI-C.

A. Validation of the Analytical Results of $P^{cov}(\lambda, T)$

For comparison, we first compute analytical results using a single-slope path loss model that does not differentiate LoS and NLoS transmissions [6]. Note that in [6], only one path loss exponent is defined and denoted by α, the value of which is $\alpha = \alpha^{NL} = 3.75$. The results of $P^{cov}(\lambda, T)$ in a sparse network
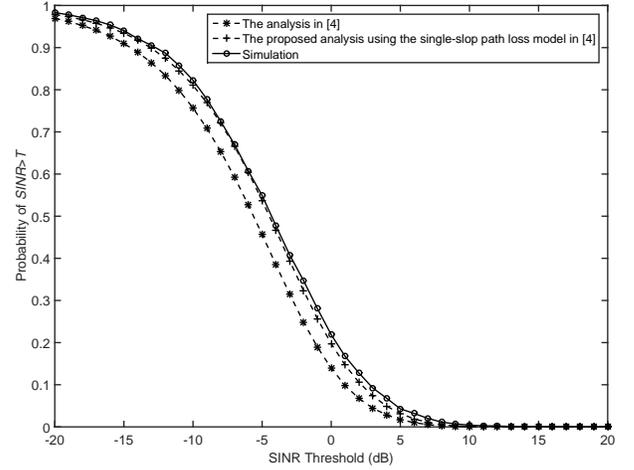
Fig. 1. The coverage probability $P^{cov}(\lambda, T)$ vs. the SINR threshold in [6] with $\lambda = 10\,\mathrm{BSs/km}^2$, $\alpha = 3.75$, and $\epsilon = 0.7$.

scenario with $\lambda = 10\,\mathrm{BSs/km}^2$, $\alpha = 3.75$, and $\epsilon = 0.7$ are plotted in Fig. 1.

In the case of the single-slope path loss model [4], as can be observed from Fig. 1, our analytical result is much more accurate than that in [6] because our system model assumptions are more reasonable than those in [6]: first, the distributions of BSs and UEs are modeled as two independent HPPPs, instead of the assumption that only UEs are distributed according to a HPPP [6]; second, the dependence of BS and UE positions are discussed, instead of being ignored [6].

In the case of the 3GPP path loss model [18], the results of $P^{cov}(\lambda, T)$ in a sparse network scenario with $\lambda = 10\,\mathrm{BSs/km}^2$ and in a dense network scenario with $\lambda = 10^3\,\mathrm{BSs/km}^2$ are plotted in Fig. 2. As can be observed from Fig. 2, our analytical results match the simulation results very well, and thus we will only use analytical results of $P^{cov}(\lambda, T)$ in our discussion hereafter.

As can be seen from Fig. 2, for the case of $\lambda = 10\,\mathrm{BSs/km}^2$, when the SINR threshold is small (e.g., $T < -4\mathrm{dB}$), the analytical result of the coverage probability is larger than the simulation result. This is because in our analysis, the approximation of replacing the location of UE by that of its serving BS, may exclude the cases of strong interfering UEs located at the proximity of the typical BS, thus underestimating the total interference, and overestimating the coverage probability. However, as the SINR threshold increases (e.g., $T > -4\mathrm{dB}$),
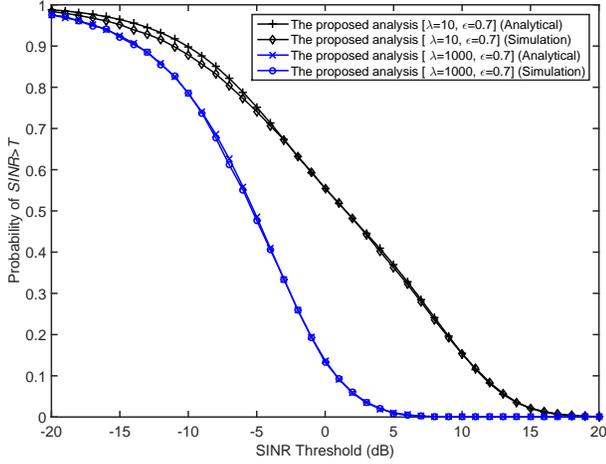
Fig. 2. The coverage probability $P^{\text{cov}}(\lambda, T)$ vs. the SINR threshold with $\lambda = 10\,\text{BSs/km}^2$ and $\lambda = 10^3\,\text{BSs/km}^2$.

Fig. 3. The coverage probability $P^{\text{cov}}(\lambda, T)$ vs. the BS density with different ϵ and SINR threshold $T = 0$ dB.

the impact of the overestimation of the coverage probability will decrease, and our analytical result matches the simulation result well.

Another interesting finding as can be observed from Fig. 2 is that the analytical result with a larger BS density is more accurate than that with a smaller BS density. This is because in denser networks, the distance between a UE and its serving BS is smaller, and the approximation of replacing the location of a UE by that of its serving BS has less impact on the estimation of the total interference, thus making the analytical result more accurate.

B. The Results of $P^{\text{cov}}(\lambda, T)$ vs. λ

The results of $P^{\text{cov}}(\lambda, T)$ against the BS density for $T = 0$ dB are plotted in Fig. 3. From Fig. 3, we can observe that when considering both LoS and NLoS transmissions, the coverage probability presents a significantly different behavior. When the SCN is sparse and thus noise-limited, the coverage probability given by the proposed analysis grows as λ increases, similarly as that observed in [6]. However, when the network is dense enough, the coverage probability decreases as λ increases, due to the transition of a large number of interference paths from NLoS to LoS, which is not captured in [6]. Particularly, during this region, interference increases at a faster rate than the signal due to the transition from mostly NLoS interference to LoS interference, thereby causing a drop in the SINR hence the coverage probability. In more detail, the coverage probability given by the proposed analysis
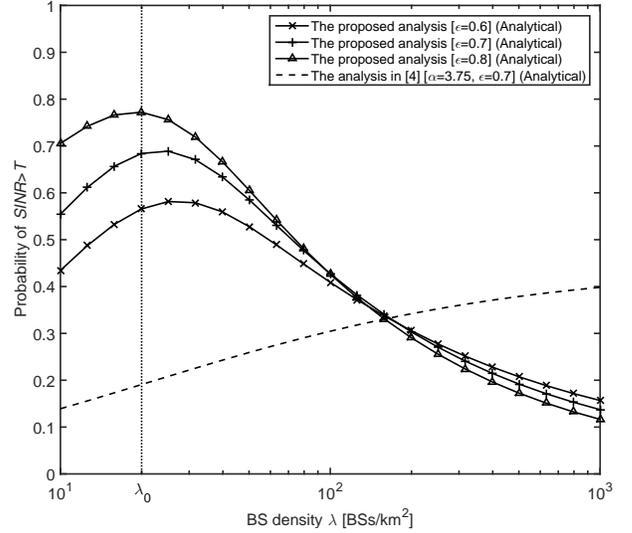
peaks at a certain density λ_0. When λ increases above λ_0, interfering UEs become closer to the typical BS and their interfering signals start reaching the typical BS via strong LoS paths. When λ is further increased far above λ_0, the coverage probability decreases at a slower pace because both the signal power and the interference power are LoS dominated and increase at approximately the same rate. There are still more and more interferers whose signal reach the typical BS via LoS paths but their effect is smaller than the dominating interferers.

It should also be noted that the coverage probability with different FPC factor ϵ exhibits different trends. Specifically, when the SCN is sparse, adopting a higher ϵ (e.g., $\epsilon = 0.8$) leads to a higher coverage probability. This is because the sparse SCN is noise-limited and hence increasing the transmission power provides better coverage performance. However, when the SCN is dense, adopting a lower ϵ (e.g., $\epsilon = 0.6$) leads to higher coverage probability. This is because the dense SCN is interference-limited, and the network experiences a surplus of strong LoS interference instead of shortage of UL transmission power, and hence decreasing the transmission power provides better coverage performance. Therefore, our results suggest that in dense SCNs, increasing the UL transmission power may degrade the coverage probability. Such observation is further investigated in terms of ASE in the following subsection.
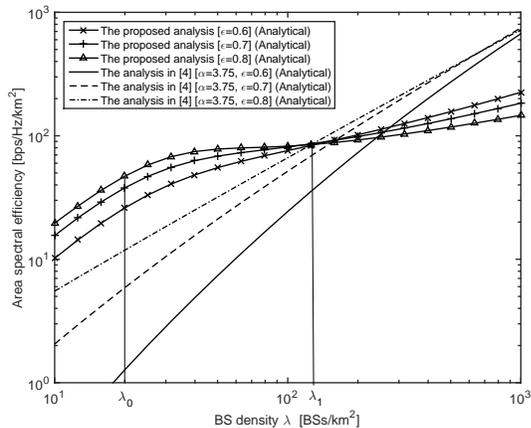
Fig. 4. Area spectral efficiency $A^{\mathrm{ASE}}\left(\lambda, T_0\right)$ vs. the BS density with different ϵ and SINR threshold $T_0 = 0$ dB. λ_0 and λ_1 correspond to the BS density when the ASE given by the proposed analysis starts to suffer from a slow growth and when it starts to pick up the growth, respectively.

C. The Results of $A^{\mathrm{ASE}}\left(\lambda, T_0\right)$ vs. λ

In this subsection, we investigate the ASE with $T_0 = 0$ dB based on the analytical results of $P^{\mathrm{cov}}\left(\lambda, T\right)$. The results of $A^{\mathrm{ASE}}\left(\lambda, T_0\right)$ obtained by comparing the proposed analysis with the analysis from [6] are plotted in Fig. 4.

As can be seen from Fig. 4, the analysis from [6] indicates that when the SCN is dense enough, the ASE increases linearly with λ. In contrast, our proposed analysis reveals a more complicated ASE trend. Specifically, when the SCN is relatively sparse, i.e., $10^0 \sim 10^1$ BSs/km^2, the ASE quickly increases with λ since the network is generally noise-limited, and thus having UEs closer to their serving BSs improves performance. When the SCN is extremely dense, i.e., around 10^3 BSs/km^2, the ASE increases linearly with λ because both the signal power and the interference power are LoS dominated. As for the practical range of λ for the existing and the future cellular networks, i.e., $10^1 \sim 10^3$ BSs/km^2 [1], the ASE trend is interesting. First, when $\lambda \in [\lambda_0, \lambda_1]$, where λ_0 is around 20 and λ_1 ($\lambda_1 > \lambda_0$) is around 125 in Fig. 4, the ASE exhibits a slow-down in the rate of growth due to the fast decrease of coverage probability shown in Fig. 3. Thereafter, when $\lambda \geq \lambda_1$, the ASE exhibits an acceleration in the growth rate due to the slow-down in the decrease of coverage probability also shown in Fig. 3. Our finding, the ASE may exhibits

a slow-down in the rate of growth as the BS density increases, is similar to our results reported for the DL of SCNs [5], which indicates the significant impact of the path loss model incorporating both NLoS and LoS transmissions. Such impact makes a difference for dense SCNs in terms of the ASE both quantitatively and qualitatively, comparing to that with a simplistic path loss model that does not differentiate LoS and NLoS transmissions.

Our proposed analysis also shows another important finding. A smaller UL power compensation factor ϵ (e.g., $\epsilon = 0.6$) can greatly boost the ASE performance in 5G dense SCNs [1], i.e., $10^2 \sim 10^3$ BSs/km^2, while a larger ϵ (e.g., $\epsilon = 0.8$) is more suitable for sparse SCNs, i.e., $10^1 \sim 10^2$ BSs/km^2. This contradicts the results in [6] where a larger UL power compensation factor was predicted to always result in a better ASE in the practical range of BS density, i.e., $10^1 \sim 10^3$ BSs/km^2, as shown in Fig. 4. Therefore, our theoretical analysis indicates that the performance impact of LoS and NLoS transmissions on UL SCNs with UL power compensation is also significant both quantitatively and qualitatively, compared with the previous work in [6] that does not differentiate LoS and NLoS transmissions. Interestingly, our new finding implies that its is possible to save UE battery and meanwhile achieve a high ASE in the UL of 5G dense SCNs, if ϵ is optimized. The intuition is that in dense SCNs, the network experiences a surplus of strong LoS interference instead of shortage of UL transmission power, and thus reducing the transmission powers of a large number of interferers turns out to be a good strategy that enhances the ASE. Note that our conclusion is made from the investigated set of parameters, and it is of significant interest to further study the generality of this conclusion in other network models and with other parameter sets.

D. Discussion on Various Values of α^{L}

In this subsection, we change the value of α^{L} from 2.09 to 1.09 and 3.09, respectively, to investigate the performance impact of α^{L}. In Fig. 5, the analytical results of $P^{\mathrm{cov}}\left(\lambda, 0\right)$ with $T_0 = 0$ dB and with various α^{L} and various ϵ are compared.

As can be seen from Fig. 5, the smaller the α^{L}, the larger the difference between the NLoS path loss exponent α^{NL} and α^{L}. As a result, performance
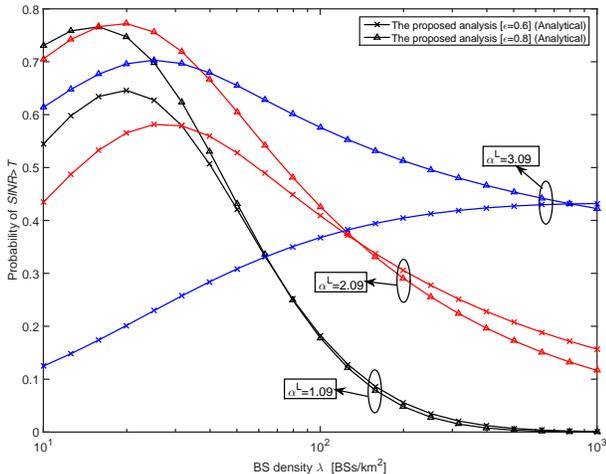
Fig. 5. The coverage probability $P^{\mathrm{cov}}\left(\lambda, T\right)$ vs. the BS density with different ϵ and α^{L}. SINR threshold $T = 0$ dB.

Fig. 6. Area spectral efficiency $A^{\mathrm{ASE}}\left(\lambda, T_0\right)$ vs. the BS density with the exponential LoS probability model, different ϵ and SINR threshold $T_0 = 0$ dB.

impact of the transition of interference from the NLoS transmission to the LoS transmission becomes more drastic as λ increases. In other words, the slow growth of the $P^{\mathrm{cov}}\left(\lambda, 0\right)$ is more obvious to observe. For example, when α^{L} takes a near-field path loss exponent such as 1.09, the decrease of the $P^{\mathrm{cov}}\left(\lambda, 0\right)$ at $\lambda \in [\lambda_0, \lambda_1]$ BSs/km^2 is substantial and it hardly recovers after λ_1.

As has been discussed in the subsection VI-B, when the SCN is sparse, adopting a higher ϵ leads to a higher coverage probability. However, as λ increases, adopting a lower ϵ leads to a higher coverage probability. The BS density around which the coverage probability with smaller ϵ surpasses that with larger ϵ is defined as the transition point of ϵ. As can be seen from Fig. 5, the transition point of various ϵ increases as α^{L} increases. It indicates that in dense SCNs with smaller α^{L}, the coverage probability using a smaller ϵ can soon outperform that using a larger ϵ as the SCN becomes denser.

E. Investigation of a Different Path Loss Model

In this subsection, we investigate the UL ASE performance assuming a more complicated path loss model, in which the LoS probability is defined as follows [18]

$$\mathrm{Pr}^{\mathrm{L}}\left(r\right) = \begin{cases} 1 - 5 \exp\left(-\frac{R_1}{r}\right), & 0 < r \le d_1 \\ 5 \exp\left(-\frac{r}{R_2}\right), & r > d_1 \end{cases}, \quad (50)$$

where $R_1 = 0.156$ km, $R_2 = 0.03$ km, and $d_1 = \frac{R_1}{\ln 10}$. The simulation results of the area spectral efficiency $A^{\mathrm{ASE}}\left(\lambda, T_0\right)$ vs. the BS density is shown in Fig. 6.

As can be seen from Fig. 6, the area spectral efficiency with the exponential LoS probability model exhibits a slow-down in the rate of growth in certain BS density regions, which qualitatively confirms our observations in subsection VI-C with the linear LoS probability model. Specifically, in Fig. 6, the numerical result for λ_0 is around 10^2 BSs/km^2. Furthermore, the area spectral efficiency with the exponential LoS probability model exhibits a similar trend as discussed in subsection VI-C with the linear LoS probability model, i.e., using a smaller UL power compensation factor ϵ can outperform that using a larger ϵ as the SCN becomes denser.

F. Investigation of the Performance Impact of Ricean Fading

In this subsection, we investigate the UL ASE performance assuming a linear path loss model including the Ricean fading. Here we adopt a practical model of Ricean fading [17] with K factor $K = 15$ dB. The simulation results of the area spectral efficiency $A^{\mathrm{ASE}}\left(\lambda, T_0\right)$ vs. the BS density is shown in Fig. 7.

As can be seen from Fig. 7, the area spectral efficiency with the linear LoS probability model and the Ricean fading exhibits a slow-down in the rate of growth as the BS density increases, which qualitatively confirms our observations in subsection VI-C for the linear LoS probability model and the Rayleigh fading. Furthermore, the area spectral
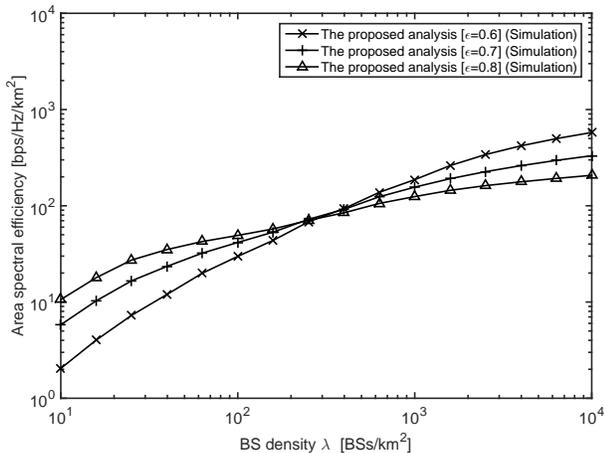
Figure 7. Area spectral efficiency $A^{\text{ASE}}(\lambda, T_0)$ vs. the BS density with the linear LoS probability model, different ϵ and SINR threshold $T_0 = 0$ dB, including the Ricean fading.

efficiency with the Ricean fading exhibits a similar trend as discussed in subsection VI-C with the Rayleigh fading, i.e., using a smaller UL power compensation factor ϵ can outperform that using a larger ϵ as the SCN becomes denser. Since the simulation results of Ricean fading and Rayleigh fading are not qualitatively different, we suggest to use a simplified model with the Rayleigh fading in theoretical analysis.

VII. CONCLUSION

In this paper, we have investigated the impact of a piecewise linear path loss model incorporating both LoS and NLoS transmissions in the performance of the UL of dense SCNs. Analytical results were obtained for the coverage probability and the ASE performance. The results show that LoS and NLoS transmissions have a significant impact in the ASE of the UL of dense SCNs, both quantitatively and qualitatively, compared with previous works that does not differentiate LoS and NLoS transmissions. Specifically, we found that

- The ASE may suffer from a slow growth as the UE density increases in the UL of dense SCNs.
- The ASE with a smaller UL power compensation factor considerably outperforms that with a larger UL power compensation factor in dense SCNs. The reverse is true for sparse SCNs.

As our future work, we will consider other factors of realistic networks in the theoretical analysis for SCNs, such as the introduction of Ricean fading or Nakagami fading, because the multi-path fading model is also affected by the LoS and NLoS transmissions.

APPENDIX A: PROOF OF THEOREM 1

Given the piecewise path loss model presented in Section III, $P^{\text{cov}}(\lambda, T)$ can be derived as

$$
\begin{aligned}
&P^{\text{cov}}(\lambda, T) \\
&= \int_0^\infty \Pr\left[\text{SINR} > T \,|\, r\right] f_R(r)\, dr \\
&= \int_0^\infty \Pr\left[\frac{P_0 g \zeta(r)^{(\epsilon-1)}}{\sigma^2 + I_Z} > T\right] f_R(r)\, dr \\
&= \int_0^{d_1} \Pr\left[\frac{P_0 g \left(A^{\text{L}} r^{\alpha^{\text{L}}}\right)^{(\epsilon-1)}}{\sigma^2 + I_Z} > T \,\middle|\, \text{LoS}\right] f_{R,1}^{\text{L}}(r)\, dr \\
&+ \int_0^{d_1} \Pr\left[\frac{P_0 g \left(A^{\text{NL}} r^{\alpha^{\text{NL}}}\right)^{(\epsilon-1)}}{\sigma^2 + I_Z} > T \,\middle|\, \text{NLoS}\right] f_{R,1}^{\text{NL}}(r)\, dr \\
&+ \ldots \\
&+ \int_{d_{N-1}}^\infty \Pr\left[\frac{P_0 g \left(A^{\text{L}} r^{\alpha^{\text{L}}}\right)^{(\epsilon-1)}}{\sigma^2 + I_Z} > T \,\middle|\, \text{LoS}\right] f_{R,N}^{\text{L}}(r)\, dr \\
&+ \int_{d_{N-1}}^\infty \Pr\left[\frac{P_0 g \left(A^{\text{NL}} r^{\alpha^{\text{NL}}}\right)^{(\epsilon-1)}}{\sigma^2 + I_Z} > T \,\middle|\, \text{NLoS}\right] f_{R,N}^{\text{NL}}(r)\, dr \\
&\triangleq \sum_{n=1}^N \left(T_n^{\text{L}} + T_n^{\text{NL}}\right).
\end{aligned}
$$
(51)

In the following, we show how to compute $f_{R,n}^{\text{L}}(r)$ and $f_{R,n}^{\text{NL}}(r)$.

To compute $f_{R,n}^{\text{L}}(r)$, we define two events as follows

Event B^{L}: The nearest BS with a LoS path to the UE is located at distance X^{L}. The CCDF of X^{L} is written as $\bar{F}_X^{\text{L}}(x) = \exp\left(-\int_0^x \Pr^{\text{L}}(u)\, 2\pi u \lambda\, du\right)$ [5]. Taking the derivative of $\left(1 - \bar{F}_X^{\text{L}}(x)\right)$ with regard to x, we can get the PDF of X^{L} as

$$
f_X^{\text{L}}(x) = \exp\left(-\int_0^x \Pr^{\text{L}}(u)\, 2\pi u \lambda\, du\right) \Pr^{\text{L}}(x)\, 2\pi x \lambda.
$$
(52)

Event C^{NL} conditioned on the value of X^{L}: Given that $X^{\text{L}} = x$, the nearest BS with a NLoS path to the UE is located farther than distance x_1, where $A^{\text{L}} x^{\alpha^{\text{L}}} = A^{\text{NL}} x_1^{\alpha^{\text{NL}}}$, and $x_1 = \left(A^{\text{L}} x^{\alpha^{\text{L}}} / A^{\text{NL}}\right)^{1/\alpha^{\text{NL}}}$. The conditional probability of C^{NL} on condition of $X^{\text{L}} = x$ can be computed by

$$
\begin{aligned}
&\Pr\left[C^{\text{NL}} \,|\, X^{\text{L}} = x\right] \\
&= \exp\left(-\int_0^{x_1} \left(1 - \Pr^{\text{L}}(u)\right) 2\pi u \lambda\, du\right).
\end{aligned}
$$
(53)

Then, we consider the event that the UE is associated with a BS with a LoS path and such BS is located at distance R_n^{L}. $f_{R,n}^{\text{L}}(r)$ can be derived as

$$f_{R,n}^{\mathrm{L}}(r)$$
$$= f_X^{\mathrm{L}}(r)\Pr\left[C^{\mathrm{NL}}\middle|\,X^{\mathrm{L}}=r\right]$$
$$= \exp\left(-\int_0^r \Pr^{\mathrm{L}}(u)\,2\pi u\lambda du\right)\Pr^{\mathrm{L}}(r)\,2\pi r\lambda$$
$$\times \exp\left(-\int_0^{r_1}\left(1-\Pr^{\mathrm{L}}(u)\right)\right.$$
$$\left.\times 2\pi u\lambda du\right), \quad (d_{n-1}<r<d_n).$$
$$(54)$$

Having obtained $f_{R,n}^{\mathrm{L}}(r)$, we move on to evaluate $\Pr\left[\dfrac{P_0 g\left(A^{\mathrm{L}}r^{\alpha^{\mathrm{L}}}\right)^{(\epsilon-1)}}{\sigma^2+I_Z}>T\middle|\,\mathrm{LoS}\right]$ in (17) as

$$\Pr\left[\frac{P_0 g\left(A^{\mathrm{L}}r^{\alpha^{\mathrm{L}}}\right)^{(\epsilon-1)}}{\sigma^2+I_Z}>T\middle|\,\mathrm{LoS}\right]$$

$$= \Pr\left[g>\frac{T\left(\sigma^2+I_Z\right)}{P_0\left(A^{\mathrm{L}}r^{\alpha^{\mathrm{L}}}\right)^{(\epsilon-1)}}\middle|\,\mathrm{LoS}\right]$$

$$= \mathbb{E}_{I_Z}\left\{\exp\left(-\frac{T\left(\sigma^2+I_Z\right)}{P_0\left(A^{\mathrm{L}}r^{\alpha^{\mathrm{L}}}\right)^{(\epsilon-1)}}\right)\right\}$$

$$= \exp\left(-\frac{T\sigma^2}{P_0\left(A^{\mathrm{L}}r^{\alpha^{\mathrm{L}}}\right)^{(\epsilon-1)}}\right)$$

$$\times \mathbb{E}_{I_Z}\left\{\exp\left(-\frac{T I_Z}{P_0\left(A^{\mathrm{L}}r^{\alpha^{\mathrm{L}}}\right)^{(\epsilon-1)}}\right)\right\}$$

$$= \exp\left(-\frac{T\sigma^2}{P_0\left(A^{\mathrm{L}}r^{\alpha^{\mathrm{L}}}\right)^{(\epsilon-1)}}\right)\mathscr{L}_{I_Z}\left(\frac{T}{P_0\left(A^{\mathrm{L}}r^{\alpha^{\mathrm{L}}}\right)^{(\epsilon-1)}}\right),$$
$$(55)$$

where $\mathscr{L}_{I_Z}(s)$ is the Laplace transform of RV I_Z evaluated at s.

To compute $f_{R,n}^{\mathrm{NL}}(r)$, we define two events as follows

Event B^{NL}: The nearest BS with a NLoS path to the UE is located at distance X^{NL}. The CCDF of X^{NL} is written as $\bar{F}_X^{\mathrm{NL}}(x) = \exp\left(-\int_0^x\left(1-\Pr^{\mathrm{L}}(u)\right)2\pi u\lambda du\right)$. Taking the derivative of $\left(1-\bar{F}_X^{\mathrm{L}}(x)\right)$ with regard to x, we can get the PDF of X^{NL} as

$$f_X^{\mathrm{NL}}(x)$$
$$= \exp\left(-\int_0^x\left(1-\Pr^{\mathrm{L}}(u)\right)2\pi u\lambda du\right) \quad (56)$$
$$\times \left(1-\Pr^{\mathrm{L}}(x)\right)2\pi x\lambda.$$

Event C^{L} conditioned on the value of X^{NL}: Given that $X^{\mathrm{NL}}=x$, the nearest BS with a LoS path to the UE is located farther than distance x_2, where $A^{\mathrm{L}}x_2^{\alpha^{\mathrm{L}}}=A^{\mathrm{NL}}x^{\alpha^{\mathrm{NL}}}$, and $x_2=\left(A^{\mathrm{NL}}x^{\alpha^{\mathrm{NL}}}/A^{\mathrm{L}}\right)^{1/\alpha^{\mathrm{L}}}$. The conditional probability of C^{L} on condition of $X^{\mathrm{NL}}=x$ can be computed by

$$\Pr\left[C^{\mathrm{L}}\middle|\,X^{\mathrm{NL}}=x\right]$$
$$= \begin{cases}\exp\left(-\int_0^{x_2}\left(\Pr^{\mathrm{L}}(u)\right)2\pi u\lambda du\right), & 0<x\le y_1\\\exp\left(-\int_0^{d_1}\left(\Pr^{\mathrm{L}}(u)\right)2\pi u\lambda du\right), & x>y_1\end{cases}.$$
$$(57)$$

Then, we consider the event that the UE is associated with a BS with a NLoS path and such BS is located at distance R_n^{NL}. $f_{R,n}^{\mathrm{NL}}(r)$ can be derived as

$$f_{R,n}^{\mathrm{NL}}(r)$$
$$= f_X^{\mathrm{NL}}(r)\Pr\left[C^{\mathrm{L}}\middle|\,X^{\mathrm{NL}}=r\right]$$
$$= \exp\left(-\int_0^r\left(1-\Pr^{\mathrm{L}}(u)\right)2\pi u\lambda du\right)\left(1-\Pr^{\mathrm{L}}(r)\right)2\pi r\lambda$$
$$\times \exp\left(-\int_0^{r_2}\left(\Pr^{\mathrm{L}}(u)\right)2\pi u\lambda du\right), \quad (d_{n-1}<r<d_n).$$
$$(58)$$

Similar to (55), $\Pr\left[\dfrac{P_0 g\left(A^{\mathrm{NL}}r^{\alpha^{\mathrm{NL}}}\right)^{(\epsilon-1)}}{\sigma^2+I_Z}>T\middle|\,\mathrm{NLoS}\right]$ can be computed by

$$\Pr\left[\frac{P_0 g\left(A^{\mathrm{NL}}r^{\alpha^{\mathrm{NL}}}\right)^{(\epsilon-1)}}{\sigma^2+I_Z}>T\middle|\,\mathrm{NLoS}\right]$$

$$= \mathbb{E}_{I_Z}\left\{\exp\left(-\frac{T\left(\sigma^2+I_Z\right)}{P_0\left(A^{\mathrm{NL}}r^{\alpha^{\mathrm{NL}}}\right)^{(\epsilon-1)}}\right)\right\}$$

$$= \exp\left(-\frac{T\sigma^2}{P_0\left(A^{\mathrm{NL}}r^{\alpha^{\mathrm{NL}}}\right)^{(\epsilon-1)}}\right)\mathscr{L}_{I_Z}\left(\frac{T}{P_0\left(A^{\mathrm{NL}}r^{\alpha^{\mathrm{NL}}}\right)^{(\epsilon-1)}}\right).$$
$$(59)$$

Our proof is completed by applying the definition of T_n^{L} and T_n^{NL} in (11).

APPENDIX B: PROOF OF LEMMA 2

Based on (21), T_1^{L} can be obtained as

$$T_1^{\mathrm{L}}$$
$$= \int_0^{d_1}\Pr\left[\frac{P_0 g\left(A^{\mathrm{L}}r^{\alpha^{\mathrm{L}}}\right)^{(\epsilon-1)}}{\sigma^2+I_Z}>T\middle|\,\mathrm{LoS}\right]f_{R,1}^{\mathrm{L}}(r)dr$$
$$= \int_0^{d_1}\exp\left(-\frac{T\sigma^2}{P_0\left(A^{\mathrm{L}}r^{\alpha^{\mathrm{L}}}\right)^{(\epsilon-1)}}\right)$$
$$\times \mathscr{L}_{I_Z}\left(\frac{T}{P_0\left(A^{\mathrm{L}}r^{\alpha^{\mathrm{L}}}\right)^{(\epsilon-1)}}\right)f_{R,1}^{\mathrm{L}}(r)\,dr.$$
$$(60)$$

The Laplace transform $\mathscr{L}_{I_Z}(s)$ is expressed as

$$\mathscr{L}_{I_Z}(s)$$
$$= \mathbb{E}_{I_Z}\left[\exp\left(-sI_Z\right)\right]$$
$$= \mathbb{E}_{r_z,d_z,g_z}\left[\exp\left(-s\sum_Z P_0\beta\left(r_z\right)\zeta\left(d_z\right)^{-1}g_z\right)\right]$$
$$= \mathbb{E}_{r_z,d_z}\left[\prod_Z \mathbb{E}_{g_z}\left(\exp\left(-sP_0\beta\left(r_z\right)\zeta\left(d_z\right)^{-1}g_z\right)\right)\right]$$
$$= \mathbb{E}_{r_z,d_z}\left[\prod_Z \frac{1}{1+sP_0\beta(r_z)\zeta(d_z)^{-1}}\right]$$
$$= \exp\left(-2\pi\lambda\int_r^\infty\left(1-\mathbb{E}_{r_z}\left[\frac{1}{1+sP_0\beta(r_z)\zeta(x)^{-1}}\right]\right)xdx\right)$$
$$= \exp\left(-2\pi\lambda\int_r^\infty\mathbb{E}_{r_z}\left[\frac{1}{1+s^{-1}P_0^{-1}\beta(r_z)^{-1}\zeta(x)}\right]xdx\right)$$
$$= \exp\left(-2\pi\lambda\int_r^{d_1}\left(1-\frac{x}{d_1}\right)\right.$$
$$\times\mathbb{E}_{r_z}\left[\frac{1}{1+s^{-1}P_0^{-1}\beta(r_z)^{-1}\zeta(x)}\Big|\text{LoS}\right]xdx\right)$$
$$\times\exp\left(-2\pi\lambda\int_{r_1}^{d_1}\left(\frac{x}{d_1}\right)\right.$$
$$\times\mathbb{E}_{r_z}\left[\frac{1}{1+s^{-1}P_0^{-1}\beta(r_z)^{-1}\zeta(x)}\Big|\text{NLoS}\right]xdx\right)$$
$$\times\exp\left(-2\pi\lambda\int_{d_1}^\infty 1\right.$$
$$\times\mathbb{E}_{r_z}\left[\frac{1}{1+s^{-1}P_0^{-1}\beta(r_z)^{-1}\zeta(x)}\Big|\text{NLoS}\right]xdx\right),\tag{61}$$

where the expectation function averaged over r_z is derived as follows

$$\mathbb{E}_{r_z}\left[\frac{1}{1+s^{-1}P_0^{-1}\beta(r_z)^{-1}\zeta(x)}\Big|\text{LoS}\right]$$
$$=\int_0^\infty\left(\frac{1}{1+s^{-1}P_0^{-1}\beta(u)^{-1}\zeta(x)}f_{R_z}(u)\,du\right).\tag{62}$$

By plugging (62) into (61), we can obtain (24).

APPENDIX C: PROOF OF LEMMA 5

By using the change of variable $\pi\lambda r^2\to\widetilde{r}$, (45) can be rewritten as

$$T_2^{\text{NL}}$$
$$=\int_{\pi\lambda d_1^2}^\infty\exp\left(-\frac{T\sigma^2}{P_0\left(\sqrt{\widetilde{r}(\pi\lambda)^{-1}}\right)^{\alpha^{\text{NL}}(\epsilon-1)}}\right)$$
$$\times\mathscr{L}_{I_Z}\left(\frac{T}{P_0\left(\sqrt{\widetilde{r}(\pi\lambda)^{-1}}\right)^{\alpha^{\text{NL}}(\epsilon-1)}}\right)e^{-\widetilde{r}}d\widetilde{r}.\tag{63}$$

By using the change of variable $\widetilde{r}-\pi\lambda\left(d_1\right)^2\to v$, (63) can be rewritten as

$$T_2^{\text{NL}}=\int_0^\infty\exp\left(-\frac{T\sigma^2}{P_0\left(\sqrt{\left[v+\pi\lambda(d_1)^2\right](\pi\lambda)^{-1}}\right)^{\alpha^{\text{NL}}(\epsilon-1)}}\right)$$
$$\times\mathscr{L}_{I_Z}\left(\frac{T}{P_0\left(\sqrt{\left[v+\pi\lambda(d_1)^2\right](\pi\lambda)^{-1}}\right)^{\alpha^{\text{NL}}(\epsilon-1)}}\right)e^{-\pi\lambda(d_1)^2}e^{-v}dv.\tag{64}$$

By using the method of Gauss-Laguerre quadrature as shown in (48), we complete the proof.

REFERENCES

[1] D. López-Pérez, M. Ding, H. Claussen, and A. H. Jafari, "Towards 1 Gbps/UE in cellular systems: Understanding ultra-dense small cell deployments," *IEEE Commun. Surveys and Tutorials*, vol. 17, no. 4, pp. 2078-2101, Fourthquarter 2015.

[2] 3GPP, "TR 36.872, Small cell enhancements for E-UTRA and E-UTRAN - Physical layer aspects," Dec. 2013.

[3] X. Ge, S. Tu, G. Mao, C.-X. Wang, and T. Han, "5G Ultra-Dense Cellular Networks," *IEEE Wireless Commun.*, vol. 23, no. 1, pp. 72-79, Feb. 2016.

[4] Xiaohu Ge, Song Tu, Tao Han, Qiang Li and Guoqiang Mao, "Energy Efficiency of Small Cell Backhaul Networks Based on Gauss-Markov Mobile Models", *IET Networks*, vol. 4, no. 2, pp. 158 - 167, 2015.

[5] M. Ding, P. Wang, D. López-Pérez, G. Mao, and Z. Lin, "Performance Impact of LoS and NLoS Transmissions in Dense Cellular Networks," *IEEE Trans. Wireless Commun.*, vol. 15, no. 3, pp. 2365-2380, Mar. 2016.

[6] T. D. Novlan, H. S. Dhillon, and J. G. Andrews, "Analytical modeling of uplink cellular networks," *IEEE Trans. Wireless Commun.*, vol. 12, no. 6, pp. 2669-2679, Jun. 2013.

[7] T. Ding, M. Ding, G. Mao, Z. Lin, and D. López-Pérez, "Uplink Performance Analysis of Dense Cellular Networks with LoS and NLoS Transmissions", *IEEE Int. Conf. Commun. (ICC)*, Kuala Lumpur, Malaysia, May 2016.

[8] J. G. Andrews, F. Baccelli, and R. K. Ganti, "A tractable approach to coverage and rate in cellular networks," *IEEE Trans. Commun.*, vol. 59, no. 11, pp. 3122-3134, Nov. 2011.

[9] X. Ge, K. Huang, C.-X. Wang, X. Hong, and X. Yang, "Capacity analysis of a multi-cell multi-antenna cooperative cellular network with co-channel interference," *IEEE Trans. Wireless Commun.*, vol. 10, no. 10, pp. 3298-3309, Oct. 2011.

[10] B. Yu, L. Yang, H. Ishii, and S. Mukherjee, "Dynamic TDD Support in Macrocell-Assisted Small Cell Architecture," *IEEE J. Sel. Areas Commun.*, vol. 33, no. 6, pp. 1201 - 1213, Jun. 2015.

[11] Anushiya Kannan, Baris Fidan and Guoqiang Mao, "Robust Distributed Sensor Network Localization Based on Analysis of Flip Ambiguities", *IEEE Global Telecommunications Conference (Globecom)*, pp.1 - 6, 2008.

[12] Ruixue Mao and Guoqiang Mao, "Road Traffic Density Estimation in Vehicular Networks", *IEEE WCNC*, pp. 4700 - 4705, 2013.

[13] Guoqiang Mao and Brian D.O. Anderson, "Graph Theoretic Models and Tools for the Analysis of Dynamic Wireless Multihop Networks", *IEEE WCNC*, pp. 1 - 6, 2009.

[14] Y. Hu, Y. Hong, and J. Evans, "Uplink Coverage and Spatial Blocking in Poisson Cellular Networks," *IEEE Int. Conf. Commun. (ICC)*, Sydney, Australia, pp. 5765 - 5770, Jun. 2014.

[15] S. Singh, X. Zhang, and J. G. Andrews, "Uplink Rate Distribution in Heterogeneous Cellular Networks with Power Control and Load Balancing," *IEEE Int. Conf. Commun. (ICC) Workshop*, London, UK, pp. 1275 - 1280, Jun. 2015.

[16] H. ElSawy, and E. Hossain, "On Stochastic Geometry Modeling of Cellular Uplink Transmission With Truncated Channel Inversion Power Control," *IEEE Trans. Wireless Commun.*, vol. 13, no. 8, pp. 4454 - 4469, Aug. 2014.

[17] J. Arnau, I. Atzeni, and M. Kountouris, "Impact of LOS-NLOS Propagation and Path Loss in Ultra-Dense Cellular Networks," *IEEE Int. Conf. Commun. (ICC)*, Kuala Lumpur, Malaysia, May 2016.

[18] 3GPP, "TR 36.828 (V11.0.0): Further enhancements to LTE Time Division Duplex (TDD) for Downlink-Uplink (DL-UL) interference management and traffic adaptation," Jun. 2012.

[19] Spatial Channel Model AHG (Combined ad-hoc from 3GPP & 3GPP2), "Subsection 3.5.3, Spatial Channel Model Text Description V6.0," Apr. 2003.

[20] C. Pozrikidis, "Numerical computation in science and engineering," New York: Oxford university press, 1998.

[21] Guoqiang Mao, Brian D. O. Anderson, Baris Fidan, "Online calibration of path loss exponent in wireless sensor networks", *IEEE Global Telecommunications Conference (Globecom)*, pp. 1 - 6, 2006.